The Company of Biologists

Cellular basis of brain maturation and acquisition of complex behaviors in salamanders

Alberto Joven[1],*, Heng Wang[1,2], Tiago Pinheiro[1], L. Shahul Hameed[1], Laure Belnoue[1] and András Simon[1],*

ABSTRACT

The overall bauplan of the tetrapod brain is highly conserved, yet significant variations exist among species in terms of brain size, structural composition and cellular diversity. Understanding processes underlying neural and behavioral development in a wide range of species is important both from an evolutionary developmental perspective as well as for the identification of cell sources with post-developmental neurogenic potential. Here, we characterize germinal processes in the brain of *Notophthalmus viridescens* and *Pleurodeles waltl* during both development and adulthood. Using a combination of cell tracking tools, including clonal analyses in new transgenic salamander lines, we examine the origin of neural stem and progenitor cells found in the adult brain, determine regional variability in cell cycle length of progenitor cells, and show spatiotemporally orchestrated neurogenesis. We analyze how maturation of different brain regions and neuronal subpopulations are linked to the acquisition of complex behaviors, and how these behaviors are altered upon chemical ablation of dopamine neurons. Our data analyzed from an evolutionary perspective reveal both common and species-specific processes in tetrapod brain formation and function.

KEY WORDS: Ependymoglia, Neurogenesis, Brain development, Behavior, Evolution, *Pleurodeles*, *Notophthalmus*, Newt

INTRODUCTION

Brain ontogeny follows an evolutionarily conserved order among vertebrates but there is a considerable diversity of brain anatomy among different species (Charvet et al., 2011; Medina and Abellan, 2009). Development includes the production of new neurons and the establishment of networks via processes that are linked to the cessation of cell proliferation. Ultimately, the maturation of a specific region is associated with the emergence of stereotypical behaviors (Arber, 2012; Fareri and Tottenham, 2016). Variations among different taxa might arise by several mechanisms, such as alterations in the timing of neurogenesis, changes in cell cycle rates, and species differences in morphogen patterning. Comparative analyses of related species have revealed some of the fixed and flexible developmental programs during vertebrate brain formation (Charvet et al., 2011; Montgomery et al., 2016). In this context, evo-devo approaches have contributed to the current understanding of how variation influences brain function and behavioral diversity across organisms, but more work across a wide diversity of species is needed (O'Connell, 2013).

[1]Department of Cell and Molecular Biology, Karolinska Institute, 17177 Stockholm, Sweden. [2]College of Animal Science and Technology, Huazhong Agricultural University, Wuhan 430070, China.

*Authors for correspondence (alberto.joven.araus@ki.se; andras.simon@ki.se)

A.J., 0000-0002-0926-4665; A.S., 0000-0002-1018-1891

Salamanders are ideally suited for studying these questions because they are the most basal branching extant clade, with high resemblance to the hypothetical common ancestor from which all tetrapods evolved (Griffiths, 1995). Although the salamander brain has undergone secondary morphological simplifications, its functional capacity is comparable to that of amniotes (Roth et al., 1993; Roth and Walkowiak, 2015). Indeed, early research performed in developing salamanders (Coghill, 1924) was instrumental in establishing a foundation for the neural basis of the ontogeny of behavior (Hamburger, 1963; Fentress, 1992). Salamanders are re-emerging as animal models not only due to their ancestral traits, but also because of their extraordinary regenerative abilities, including the brain (Amamoto et al., 2016; Berg et al., 2010; Hameed et al., 2015; Kirkham et al., 2014; Maden et al., 2013; Parish et al., 2007). In contrast to other non-mammalian vertebrate model organisms, little is known about the proliferation patterns, glial diversity and neurogenesis in the formation of the salamander brain (Barbosa et al., 2015; D'Amico et al., 2011; Ganz and Brand, 2016; Kaslin et al., 2008; Nomura et al., 2013, 2016; Raucci et al., 2006; Thuret et al., 2015; Watanabe et al., 2015; Wullimann et al., 2005; Zupanc et al., 2005). In this work we focused on the developing and adult brain of two laboratory model salamander species, the Spanish ribbed newt [*Pleurodeles waltl* (*Pw*)] and the red spotted newt [*Notophthalmus viridescens* (*Nv*)], which have an estimated 60 million years of divergence (www.timetree.org).

A distinctive feature of the salamander brain is the persistent presence of radial glia-like ependymoglia that line the ventricular system. Similar to radial glia in mammals, salamander ependymoglia have neurogenic potential and their activation is a key step in injury-induced neurogenesis in the adult brain (Berg et al., 2011). In adult *Notophthalmus*, two ependymoglia populations were previously defined: type 1 cells with stem cell properties; and type 2 cells, which have characteristics of transit amplifying progenitors (Kirkham et al., 2014). Here, we explored the origin and properties of these ependymoglial subpopulations during development in defined anatomical regions. We carried out a comprehensive study of the acquisition of quiescence and brain maturation during development. Using nucleotide pulse-chase experiments along with clonal analyses in transgenic animals we show that the cell cycle lengths vary in different brain regions in a time- and species-specific manner. We reveal a correlation between the appearance of regions with low germinal activity in both species, ependymoglial maturation and increasing cell cycle length. Further, we show temporal-specific patterns of neurogenesis in different brain areas linked to the acquisition and refinement of feeding and locomotor behaviors.
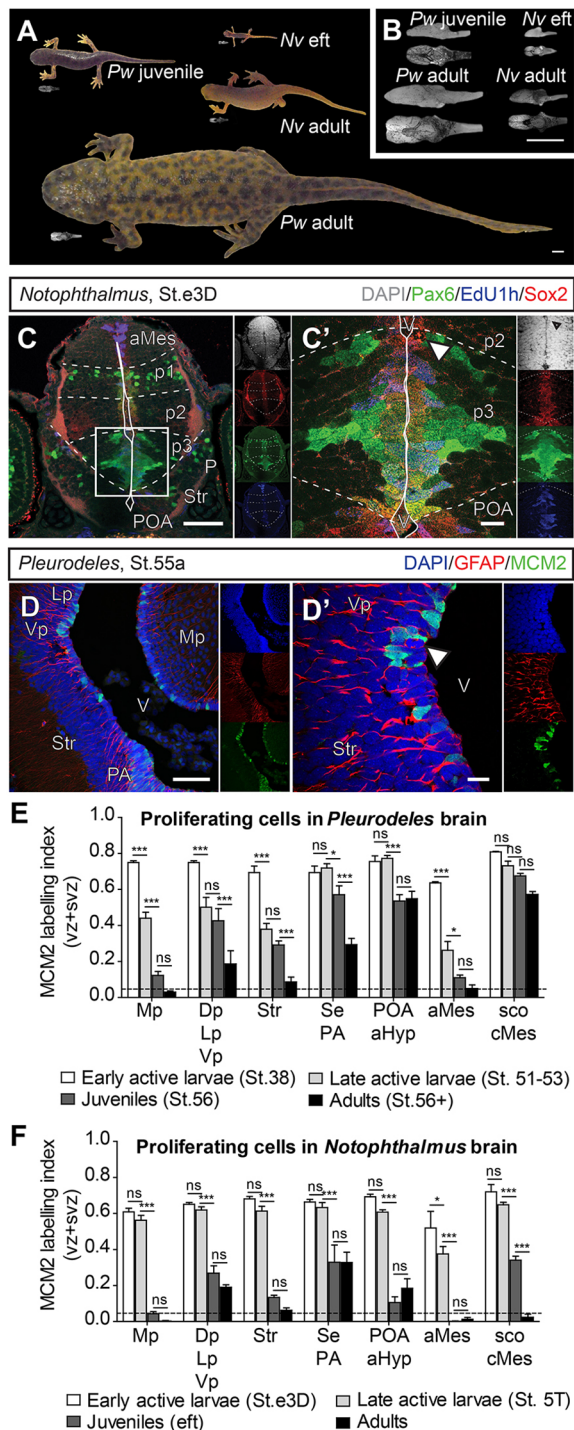
RESULTS

Proliferation rates decrease in a species-specific manner

In absolute terms, *Pleurodeles* has a larger brain than *Notophthalmus*, but relative to body size *Notophthalmus* has a larger brain than *Pleurodeles* (Fig. 1A,B). First, we confirmed that the regionalization

DEVELOPMENT

Fig. 1. Proliferation during brain development of two salamander species.
(A) Juvenile and adult *Pleurodeles* and *Notophthalmus* and corresponding dissected brain. (B) Sagittal and dorsal views of the brains depicted in A at higher magnification. (C) Transverse sections of a *Notophthalmus* early active larval brain (stage e3D) at the level of the diencephalon/telencephalon, showing the expression of key transcription factors: *Sox2* is expressed in all VZ/SVZ cells, whereas *Pax6* expression highlights boundaries between regions. (C′) High magnification of the inset in C (arrowhead points to a mitotic figure). Continuous lines delineate the ventricles, dashed lines separate prosomeres. (D) Transverse sections of a *Pleurodeles* late active larval brain (stage 55a) at the level of the telencephalon, showing the expression of GFAP in proliferating (MCM2$^+$) ependymoglial cells among VZ/SVZ cells. (D′) High magnification of the inset in D (arrowhead points to a mitotic figure). (E,F) Quantification of proliferating cells at four representative developmental stages in seven representative brain regions for *Pleurodeles* (E) and *Notophthalmus* (F). Despite the general trend of decreasing proliferation during development, the dynamics are region and species specific. Quiescence is defined as less than 5% of MCM2$^+$ cells in the VZ/SVZ (represented in the bar charts as a dashed line). Source data are provided in Tables S2 and S3. Two-way ANOVA with Bonferroni post-hoc test; *$P<0.05$, **$P<0.01$, ***$P<0.001$; ns, not significant. Mean±s.e.m. aHyp, alar hypothalamus; aMes, alar mesencephalon; cMes, caudal mesencephalon; Di, diencephalon; Dp, dorsal pallium; Lp, lateral pallium; *Nv*, *Notophthalmus viridescens*; Mp, medial pallium; olf, olfactory organ; PA, pallidum; P, pallium; *Pw*, *Pleurodeles waltl*; POA, preoptic area; p1-3, prosomeres 1-3; Se, septum; Str, striatum; sco, subcommisural organ; V, ventricle; Vp, ventral pallium. Scale bars: 500 μm (A,B), 100 μm (C,D), 20 μm (C′,D′).
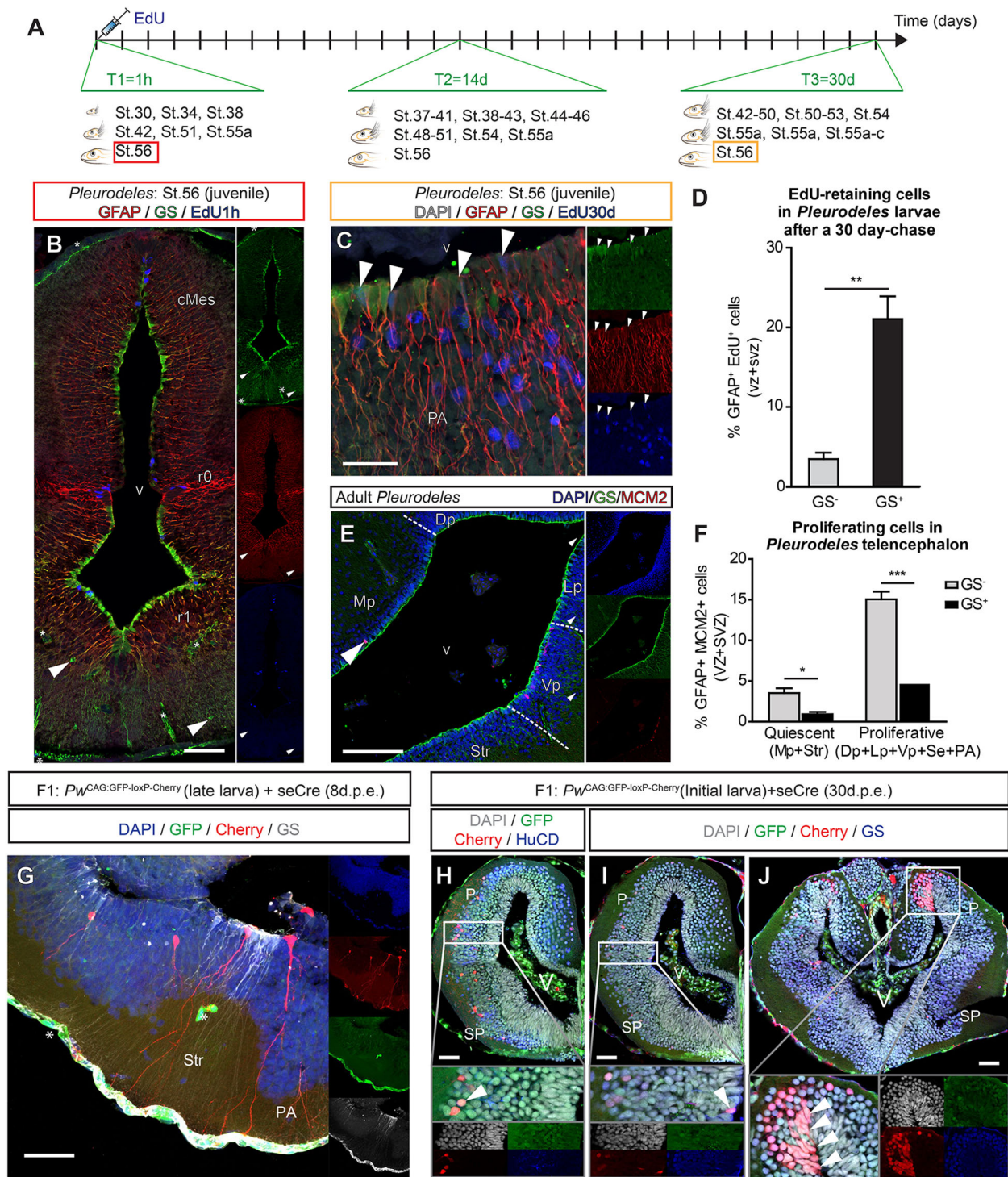
Representative stages of development were selected according to the main events that characterize the larval period in salamander development (Joven et al., 2015), and the proportion of proliferating cells in VZ/SVZ was then systematically analyzed (Fig. 1E,F, Figs S1 and S2). Similar patterns were observed in both species along development: massive proliferation characterized the initial larval period, and from the active larval period onwards quiescent regions, which are defined as ≤5% MCM2 labeling index, gradually appeared in a caudal-to-rostral direction in both species (Fig. S1). Nevertheless, *Pleurodeles* showed a higher MCM2 labeling index both during developmental stages and in the adult compared with *Notophthalmus* (Fig. S2). In the adult *Pleurodeles* brain only 4 out of 12 regions were quiescent (Fig. S2), in contrast to the adult *Notophthalmus* brain where 7 out of 12 regions were quiescent (Fig. S2). These results highlight divergent, region-specific proliferation dynamics during brain formation in two salamander species.

Ependymoglial maturation correlates with the acquisition of quiescence and the formation of sulci

In the adult *Notophthalmus* brain, two populations were previously defined among proliferating ventricular ependymoglial cells, which can be distinguished by the expression of glutamine synthetase (GS). Type 1 cells, which are GFAP$^+$/GS$^+$, are the main proliferating cell type in the quiescent areas, whereas type 2 ependymoglia cells, which are GFAP$^+$/GS$^-$, represent the vast majority of progenitors in proliferating areas (Kirkham et al., 2014). We explored the appearance and properties of these subpopulations during development by means of EdU pulse-chase experiments (Fig. 2A).

We observed consistent patterns among larvae according to their developmental stage. First, we confirmed in *Pleurodeles* that, 1 h after EdU pulsing, the highly proliferative regions (see Figs S1 and S2) were enriched in GFAP$^+$/EdU$^+$ cells (Fig. 2B). At early stages, all VZ/SVZ ependymoglial cells corresponded to type 2 cells (GS$^-$) (Fig. S3A). As the ependymoglia mature, we could distinguish two subpopulations based on GS expression (Fig. S3B,C). Fig. S3D shows the temporal appearance of GS$^+$ cells in the different brain regions. We found that

of the *Notophthalmus* brain is similar to that published for *Pleurodeles* (Joven et al., 2013a,b) in terms of cytoarchitecture and transcription factor expression patterns (Fig. 1C). We carried out combinatorial staining for the proliferation marker minichromosome maintenance protein 2 (MCM2), nucleotide incorporation [using 5-ethynyl-2′-deoxyuridine (EdU)] and expression of the ependymoglial cell markers Sox2 and glial fibrillary acidic protein (GFAP) (Kirkham et al., 2014). We observed that proliferation was largely restricted to the Sox2$^+$/GFAP$^+$ cells in the ventricular zone (VZ) and subventricular zone (SVZ) for both species (Fig. 1C,D); scattered cells were sparsely detected in the mantle zone (MZ) and in the fiber zone.

Fig. 2. Acquisition of quiescence correlates with the emergence of GS expression in ependymoglial cells. (A) Thymidine analog pulse-chase timeline and the developmental stages (St.) analyzed (*n*=4 per group and time point). (B) Thymidine analog incorporation after 1 h showed that actively proliferating ventricular patches correspond to GS⁻ ependymoglial cells. Note that the basal processes of the GS⁺ ventricular cells are covering the blood vessels and the pia mater (asterisks). Only a few GS⁺/GFAP⁻ cells are found in the parenchyma (arrowheads). (C,D) After 30 days chase, the GS⁺ ependymoglial cells retain more EdU than GS⁻ ependymoglial cells. The arrowheads point to GS⁺/EdU⁺ double-labeled cells. Student's *t*-test (two tailed), **P=0.001. Mean±s.e.m. Source data in Table S4. (E,F) Even if most of the ependymoglial cells in the adult *Pleurodeles waltl* telencephalon are GS⁺, the majority of MCM2⁺ cells were GS⁻. The arrowhead points to a GS⁺/MCM2⁺ double-labeled cell. Two-way ANOVA with Bonferroni post-hoc test; *P<0.05, ***P<0.001. Mean±s.e.m. Source data in Table S5. (G-J) Electroporation of *seCre* in *Pw^GFP-loxp-Cherry* allows permanent labeling of ependymoglia and their progeny. Eight days after electroporation, individual ventricular and parenchymal cells are distinguishable. Note the contact of ependymal glia cell radial processes with the blood vessels and pial surface (asterisks), as highlighted by the higher GFP signal in those structures (G). Representative images of HuC/D and GS labeling 30 days after electroporation, in which arrowheads highlight newly born neurons (H), quiescent progenitors (I) and expanding ependymoglia and their progeny (J). Electroporation conditions in Tables S7 and S8. d.p.e., days postelectroporation. r0, isthmus; r1, rhombomere 1; SP, subpallium; other labels as Fig.1. Scale bars: 50 µm (C), 100 µm (B,G-J), 200 µm (E).

DEVELOPMENT

the GS⁺ cells are associated with sulci, which anatomically separate brain regions as exemplified by the pallium-subpallium boundary (Fig. S3B). These observations highlight a relationship between the quiescent sulci and the actively proliferating emerging bulges. These data also indicate that GS⁻ ependymoglial cells are highly proliferative and that GS⁺ ependymoglial cells are largely quiescent.

We next analyzed the EdU-chased cells 14 and 30 days after injection in *Pleurodeles* larvae of different stages (Fig. 2A,C,D). In regions where GS⁺ cells first appear, we detected more EdU-retaining cells in the VZ/SVZ (Fig. 2C,D). By contrast, in GS⁻ highly proliferative regions, we found more EdU-labeled cells in the parenchyma and decreasing EdU signal intensity in the cells lining the ventricle (Fig. 2C).

In order to compare with the previous report on adult *Notophthalmus* (Kirkham et al., 2014), we quantified the percentage of type 1 and type 2 cells expressing MCM2 in the adult *Pleurodeles* telencephalon (Fig. 2E,F). In contrast to adult *Notophthalmus*, type 2 cells are the main proliferating subpopulation in both proliferating hotspots and quiescent regions in adult *Pleurodeles* (Fig. 2E,F), and also in developing *Notophthalmus* (Fig. S3E,F).

Next, we wanted to corroborate the conclusions of the nucleotide pulse-chase experiments with purpose-made transgenic newts carrying the conditional reporter *CAG:loxp-GFP-loxp-Cherry*. Founders (F0) were mosaic animals that were bred with wild types, and the resulting F1 larvae were screened by selecting the green fluorescent progeny carrying the transgene (*Pw^GFP-loxp-Cherry*) (Fig. S4A,B). We noted that, similar to previous reports in mice (Takeuchi et al., 2003), the CAG promoter drives GFP expression ubiquitously but with differing efficiency depending on the cell type. We developed a protocol for brain electroporation in larvae (Fig. S4C,D) in order to express self-excising *Cre* (*seCre*; Loulier et al., 2014), which resulted in a selective *Cherry* labeling of ependymoglial cells that could be detected after 48 h (Fig. S4E). Cherry was detected neither in the absence of *seCre* electroporation nor after electroporation with a control plasmid (Fig. S4F). This method allowed us to permanently label a fraction of the ependymoglia and all their progeny. Eight days after electroporation we detected Cherry-labeled cells in the parenchyma, showing that some of the ependymoglia progeny had exited the VZ/SVZ zone, probably representing differentiating neurons (Fig. 2G). We also found that blood vessels and meninges retained strong GFP labeling, highlighting the close contact of these structures with the ependymoglia processes (Fig. 2G). Thirty days after electroporation we detected both individual (Fig. 2H,I) as well as densely packed cells in all layers (Fig. 2J). We determined the identity of the labeled cells by their morphology, position and expression of cell type-specific markers: HuC/D for neurons (Fig. 2H) and GS for ependymoglia (Fig. 2I,J). We found that GS⁺/Cherry⁺ cells were isolated, whereas GS⁻/Cherry⁺ cells were grouped together. These findings support the conclusion that GS⁺ are quiescent whereas GS⁻ ependymoglia are actively proliferating.

Cell cycle length correlates with the acquisition of quiescence
Whether the cell cycle length varies between regions and species during development remained an open question. We measured cell cycle length at the population level by sequential injection of the nucleotide analogs EdU and BrdU (Martynoga et al., 2005; Nowakowski et al., 1989) (Fig. 3A, Fig. S5A-D). Whereas the length of S-phase was estimated to be constant among regions in both species (Fig. S5E), the entire length of the cell cycle varied significantly. It was stable in initial larvae across all examined

regions, although longer in *Pleurodeles* than in *Notophthalmus* (Fig. 3B,C). However, regions that were becoming quiescent harbored more slowly cycling populations in late larvae of both species (Fig. 3B,C). Notably, the pallium showed a significant increase in cell cycle length only in *Pleurodeles*. This difference is in accordance with data showing that the telencephalon of *Notophthalmus* has not yet started to become a quiescent region in late active larvae (Fig. S2B). These results show that extension of cell cycle length during brain formation is a conserved trait in salamanders. The data also highlight that the exact length of the cell cycle and the pattern of its changes are species and region specific.

The cell cycle length measurements were carried out at the population level. In order to attain resolution at the cellular level, we carried out clonal analyses by implementing the multiaddressable genome-integrative color (MAGIC) system developed by Loulier and collaborators (Loulier et al., 2014). In this system, *seCre*-mediated recombination results in a random combination of different fluorescent proteins with distinct emission spectra. We generated transgenic *Pleurodeles* expressing a combination of *Nucbow* (nuclear label) and *Cytbow* (cytoplasmic label). We electroporated *seCre* into the F1 larvae (*Pw^NucCyt*). Cre protein was detected as early as 22 h after electroporation and restricted to VZ/SVZ (Fig. S6A). No recombination occurred without Cre expression, and Cre was no longer detected by immunohistochemistry 5 days after electroporation (Fig. S6B,C). We analyzed brains at different stages of development 15 days after *seCre* electroporation. Clones located in quiescent areas remained as local, small clusters close to the VZ/SVZ (striatum in Fig. 3D, suprachiasmatic nucleus in Fig. 3E), whereas clones belonging to expanding regions were composed of more cells spreading into the MZ (pallium in Fig. 3D, paraventricular area in Fig. 3E). Next, we compared the number of daughter cells belonging to individual clones in regions that are becoming quiescent with those that will remain proliferative in the developing larvae. Clones located in proliferating regions were composed of tenfold more cells than clones located in quiescent areas (Fig. 3E,F). In addition, analyses of individual clones revealed several migratory patterns in terms of both distance from the VZ/SVZ and clone density: some clones were detected as densely packed cell groups, whereas others showed a salt-and-pepper pattern (Fig. 3G-I). This illustrates the progenitor diversity in the salamander brain. The estimation of cell cycle length at the population level together with the clonal analyses confirmed the conclusion that GS⁺ ependymoglia are slowly dividing progenitors.

Spatiotemporally defined neurogenesis correlates with the acquisition of feeding and locomotor behaviors
In order to address neurogenic programs in the newt brain we first analyzed the expansion of the telencephalon during *Pleurodeles* development (Fig. 4A-C). We used Sox2 as a marker of ependymoglial cells and NeuN as a marker of mature neurons (Fig. 4A,B). Next, we carried out EdU pulse-chase experiments and measured the distance of EdU-chased cells from the ventricle 30 days after pulsing at three representative stages in developing *Pleurodeles*. The positions occupied by labeled cells should be related to the thickness of the cytoarchitectural domains shown in Fig. 4B. When animals were pulsed during the embryonic (i.e. pre-larval) period, very few chased cells were found in the VZ/SVZ, and most of the labeled cells were located in neuronal layers (Fig. 4C, green dots). By contrast, pulsing active larvae showed a progressive accumulation of EdU-retaining cells in the VZ/SVZ (Fig. 4C, cyan and blue dots). The location of newborn cells during the different developmental periods illustrates the regional peaks of neurogenesis, which correlated with increased complexity of
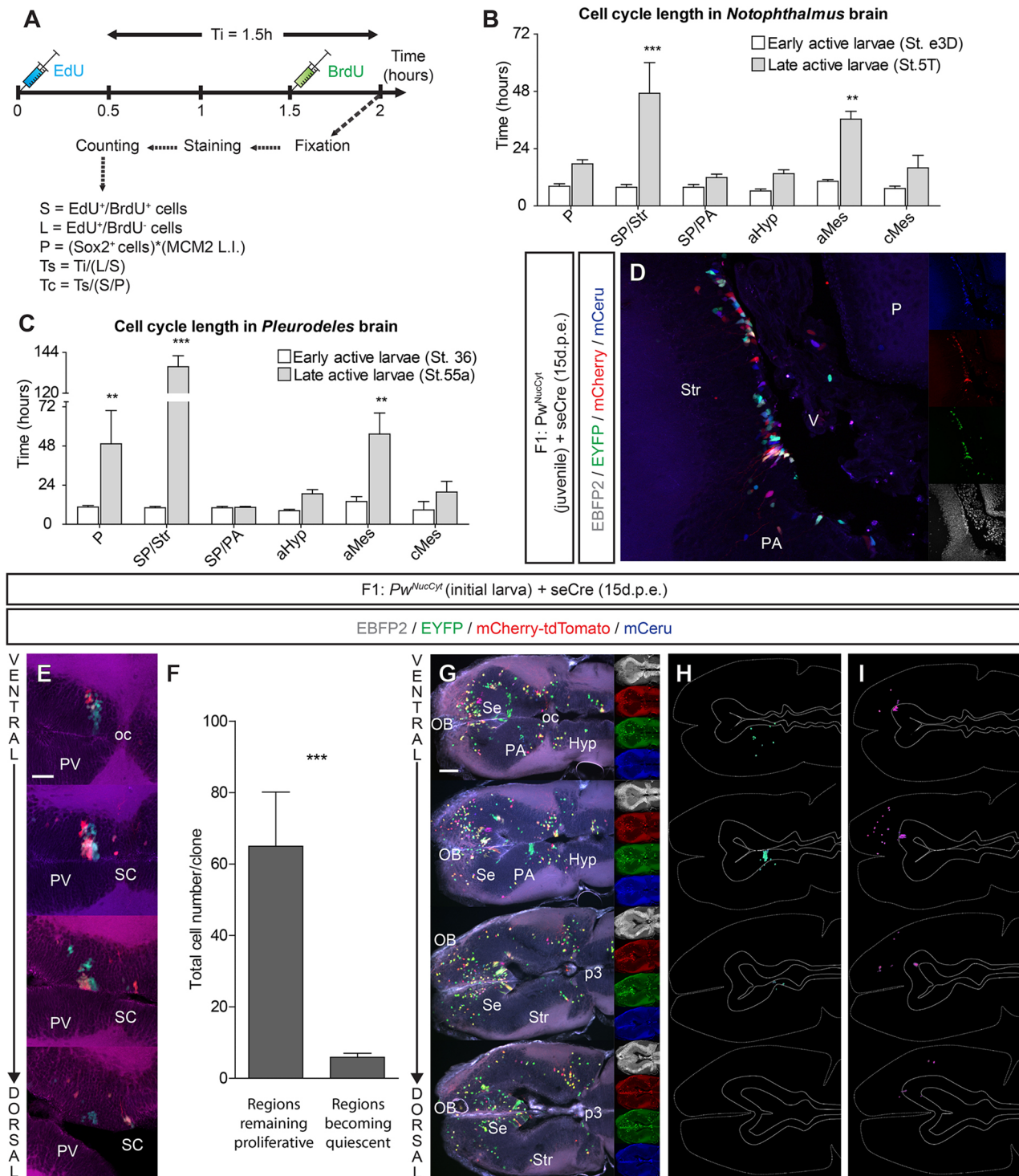
Fig. 3. Cell cycle length varies regionally in a species-specific manner. (A) Experimental design to compare cell cycle length by sequential injection of thymidine analogs. See Materials and Methods for explanation of terms. (B,C) In early active larvae, all regions are similar in both species in terms of cell cycle length. In late active larvae, *Pleurodeles* in general display a longer cell cycle than *Notophthalmus*. The cell cycle in late active larvae is prolonged in regions that are becoming quiescent (striatum, alar mesencephalon). The cell cycle in the pallium is significantly prolonged in late active larvae only in *Pleurodeles* but not in *Notophthalmus*. Two-way ANOVA with Bonferroni post-hoc test; **$P<0.01$, ***$P<0.001$. Mean±s.e.m. (D-I) Electroporation of *seCre* in Pw^{NucCyt} reveals clonally related individual cells. Those located in quiescent areas remain as local small clusters, mainly close to the VZ/SVZ (striatum in D, suprachiasmatic nucleus in E), whereas clones belonging to expanding regions are composed of more cells spreading into the parenchyma (pallidum in D, paraventricular area in E). Clones in regions remaining proliferation are composed of significantly more cells than clones in regions that are becoming quiescent (F). Student's *t*-test (two tailed); ***$P<0.001$. Mean±s.e.m. Image illustrating a variety of migratory patterns in the developing *Pleurodeles* brain (G). Examples of individual clones with different migratory patterns in terms of distance from the VZ/SVZ (longer in H than I), direction (topologically towards lateral and ventral in H; and towards rostral and dorsal in I), and clone density. The dashed line indicates the outline of the section and the continuous lines delineate the VZ/SVZ (H,I). Source data in Tables S16-S18. Electroporation conditions in Tables S9 and S10. Hyp, hypothalamus; OB, olfactory bulb; oc, optic chiasma; PV, paraventricular area; SC, suprachiasmatic nucleus; other labels as Figs 1 and 2. Scale bars: 100 µm (D,E), 200 µm (G).
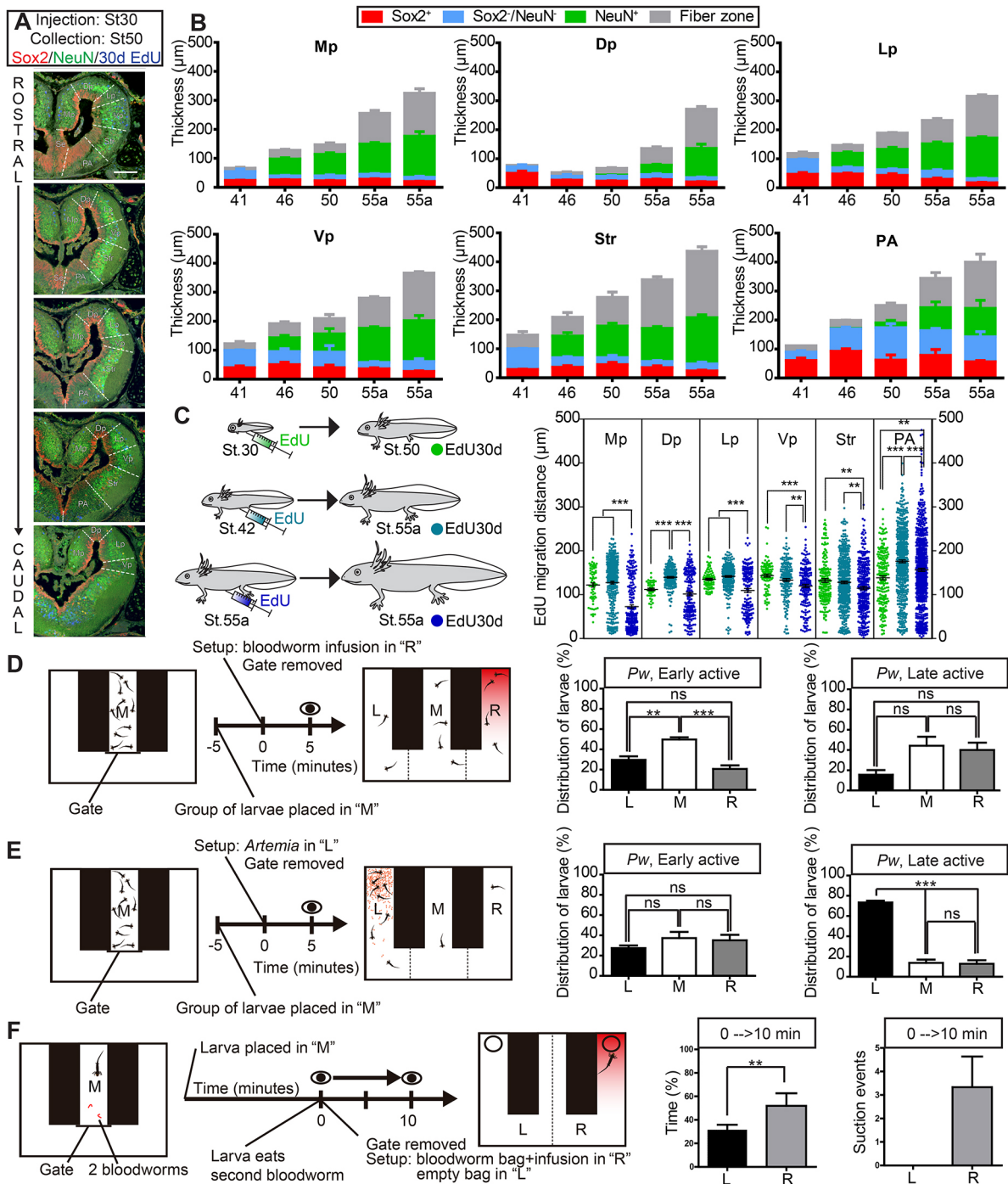
DEVELOPMENT

5

Fig. 4. See next page for legend.

feeding and locomotor behaviors (see below). We could conclude that striatum and medial pallium mature first, followed by lateral and ventral pallia, with dorsal pallium and pallidum development occurring last (Fig. 4B,C).

In *Notophthalmus* (Fig. S7A-E), we detected NeuN⁺ cells throughout the brain as early as the initial larval period (Fig. S7B), and observed a substantial increase in the number of neurons at subsequent stages (Fig. S7C). Four days after EdU pulsing of initial larvae, some of the EdU-chased cells were found to be proliferating cells whereas others had exited the proliferating VZ/SVZ and were labeled by phosphohistone H3 (PH3) and MCM2 (Fig. S7D). By contrast, in the active larval period, the EdU-

labeled cells were mainly located in the VZ/SVZ (Fig. S7E). Thirteen days after EdU injection, the chased cells were further from the VZ/SVZ in the initial larvae as compared with the active larvae (Fig. S7D,E), and some were EdU⁺/NeuN⁺ double positive (arrows, Fig. S7B,C). Interestingly, only a few of these newborn neurons were detected in the more mature areas where GS⁺ and NeuN⁺ cells appear first. Instead, they were more abundant in expanding regions (e.g. compare rhombencephalon, dorsal midbrain and pallium in Fig. S7B,C). These results show that, as in *Pleurodeles*, the production rate of newborn neurons in *Notophthalmus* is directly linked to proliferative activity (and therefore ependymoglial maturation) in a stage- and region-specific manner.

Fig. 4. Neurogenesis in larval telencephalon and the acquisition of stereotypical behaviors. (A) Representative serial sections used for quantifying the thickness of the different layers. (B) Thickness of the different cytoarchitectural domains (VZ/SVZ, Sox2^{+}/NeuN[−]; intermediate, Sox2^{−}/NeuN[−]; neuronal, Sox2^{−}/NeuN[+]; and fiber layers) along the dorsal-ventral and rostral-caudal axes in six defined regions (medial, dorsal, lateral and ventral pallia, striatum and pallidum), showing the appearance of NeuN^{+} cells and the thickening of neuronal and fiber layers. The numbers on the x-axis represent developmental stages. Error bars represent the variability along the rostral-caudal axis. A wave of neurogenesis occurs first in medial pallium and striatum, detected by stage 46. At this stage, the lateral and ventral pallia also contain a noticeable neuronal layer that gradually increases in late active larvae. The pallidum shows its first neurons at stage 50. Dorsal pallial neurogenesis occurs last, mainly during stage 55a. (C) After a 30 day EdU chase period the position of the EdU-retaining cells illustrates that the gradual decrease in migration distance during neurogenesis during development is region specific. Each dot represents one cell from three animals per stage pooled together. (D) Olfaction was assessed by counting the spatial distribution of groups of larvae in a tank divided into three chambers 5 min after opening the gate and releasing the olfactory stimulus. Whereas early active larvae show no preference for either chamber L or R, 3 cm late active larvae prefer the chamber with the smell of food. (E) Stimulus response-learning was tested using the same type of setup as in D but with live food, which animals were fed with from the start of the early active larval period (see Movie 1). Whereas early active larvae show an even distribution in the tank, 3 cm late active larvae remain in the part of the tank that contains food, displaying exploratory behavior. This motivational modulation of locomotor behavior shows the onset of instrumental conditioning in salamander larvae. (F) Olfaction-driven exploratory and feeding behaviors measured in 5 cm late active larvae during 10 min. Larvae spend more time in the chamber with the olfactory stimulus and displaying exploratory behavior, and most of them display suction feeding behavior only in that chamber (see Movie 2), showing that the olfactory information is used in associative learning for a complex foraging behavior. (C-E) One-way ANOVA with Newman-Keuls post-hoc test; **$P<0.01$, ***$P<0.001$. Mean±s.e.m. (F) Student's t-test (two tailed); **$P<0.01$. Mean±s.e.m. Source data in Tables S19-S27. L, left; M, middle; R, right; other labels as Fig. 1. Scale bar: 200 µm (A).

The maturation of the forebrain was then compared with the acquisition of stereotyped behaviors. At stage 41 (early active larval period), feeding occurs through reflex suction triggered by visual and vibrational stimuli and the larvae remain motionless unless an escape response is evoked (Movie 1). At this point of development, neither larvae showed preferences for olfactory cues nor active exploratory behavior for prey catching (Fig. 4D,E). We could not detect mature neurons in the telencephalon based on NeuN expression at this developmental stage (Fig. 4B). Nevertheless, at the end of the early active larval period (stage 45), the animals displayed a combination of walking, swimming, lunging and suction during active hunting behavior (Movie 1). This emergence of behaviors relates to the maturation of striatum and medial pallium. We detected neurons and measured a thickening of the fiber zone at stage 46 (Fig. 4B) in several telencephalic areas (medial, lateral, ventral pallia, and striatum), which correlated with the acquisition of active hunting-foraging, the first use of olfaction (olfaction test, Fig. 4D) and motivational modulation of locomotor behavior in feeding (stimulus-response learning test; Fig. 4E, Movie 1). NeuN^{+} cells appear in the dorsal pallium and the pallidum from stage 50 (Fig. 4B), which correlates with the modulation of olfaction-driven exploratory and feeding behavior in larger late active larvae (Fig. 4D,F, Movies 1 and 2).

Diverse subpopulation dynamics in dopaminergic and cholinergic neurogenesis

We next focused on the maturation of different subpopulations of the dopaminergic and cholinergic systems, as these systems have been implicated in the neural control of locomotor behaviors (Dannenberg et al., 2016; Swart et al., 2017) and more complex brain functions, such as associative learning, decision making, fear and reward

systems (Abraham et al., 2014; Hiebert et al., 2014; Levita et al., 2002; Martinez et al., 2008). We used antibodies against tyrosine hydroxylase (TH) to detect dopamine neurons, against Nkx6.1 to identify cholinergic progenitors, and against choline acetyltransferase (ChAT) to detect mature cholinergic neurons. *Pleurodeles* larvae at different stages were also pulsed with EdU as described in Fig. 2A in order to label the progeny of the ependymoglia in subtype-specific neurogenesis. We found Nkx6.1[+]/EdU[+], ChAT[+]/EdU[+] and TH[+]/EdU[+] after 14 days chasing in all the stages (Fig. 5A,B, Fig. S8A). Cells with strongest immunoreactivity for the neuronal markers were never positive for EdU, suggesting that they were born before EdU injection (Fig. 5A,B). In the case of the ventral midbrain, EdU[+]/TH^{+} cells were always found in the most caudal sections independent of the stage of injection (Fig. 5A,B), suggesting a caudal-to-rostral origin of this group. Very few EdU[+]/TH[+] or EdU[+]/ChAT^{+} cells were observed after analyzing post-metamorphic *Pleurodeles* chased for 30 days compared with larval stages, suggesting that dopaminergic and cholinergic neurogenesis slowed down but is still present in juveniles (data not shown). We then performed stereological quantification of defined subpopulations in both species starting from the early active larval period. Total cell number increased until adulthood, but the growth dynamics varied among subpopulations and species (Fig. 5C, Fig. S8B-D, Fig. S9). In general, *Pleurodeles* showed higher numbers of TH[+] and ChAT[+] cell bodies than *Notophthalmus* during larval stages (Fig. 5C, Fig. S8B, Fig. S9). Although one would expect that the bigger brain of adult *Pleurodeles* should have more mature neurons in all the subpopulations, this was not the case (Fig. 5C, Fig. S8B, Fig. S9). We observed statistically significant sexual dimorphism in terms of total TH[+] cell number for several dopaminergic groups in *Pleurodeles* (olfactory bulbs, preoptic area, suprachiasmatic nuclei and ventral midbrain) (Fig. 5C, Fig. S9A-D). For the other subpopulations, and in all subpopulations in *Notophthalmus*, there was no difference in the number of neurons between males and females (Fig. S9).

Cellular and behavioral consequences of dopaminergic neuron ablation during larval development

Next, we explored the functional role of developmental dopaminergic neurogenesis by performing behavioral tests following selective ablation of dopaminergic neurons. In accordance with our previous data on adult *Notophthalmus* (Parish et al., 2007), intraventricular injection of the neurotoxin 6-hydroxydopamine (6-OHDA) into *Pleurodeles* larvae caused the selective death of dopamine neurons in the midbrain as well as their projections to the forebrain (Fig. 6A,B, Fig. S10A,B). To assess conditional learning we performed a stimulus-response learning test as described in Fig. 4E. To our surprise, more animals were found in the chamber containing *Artemia* in the lesioned groups (Fig. 6C). We hypothesized that this might be due to reduced fear mediated by the dopaminergic system in the nucleus accumbens (Levita et al., 2002; Martinez et al., 2008). Indeed, the injured larvae were more prompted to explore the new environment even in the absence of cues (Fig. 6D).

To test the involvement of striatal dopamine in the decision-making capacity of lesioned animals, we measured suction events in the olfaction-driven foraging test as described in Fig. 4F. The lesioned animals showed a fourfold increase in suction events compared with the controls (Fig. 6E). Our data indicate that in salamanders forebrain dopaminergic innervation from the midbrain is involved in cognitive functions, including instrumental learning, fear processing and decision making.

Our previous data showed that adult *Notophthalmus* restore the midbrain dopaminergic system following ablation (Berg et al.,

DEVELOPMENT
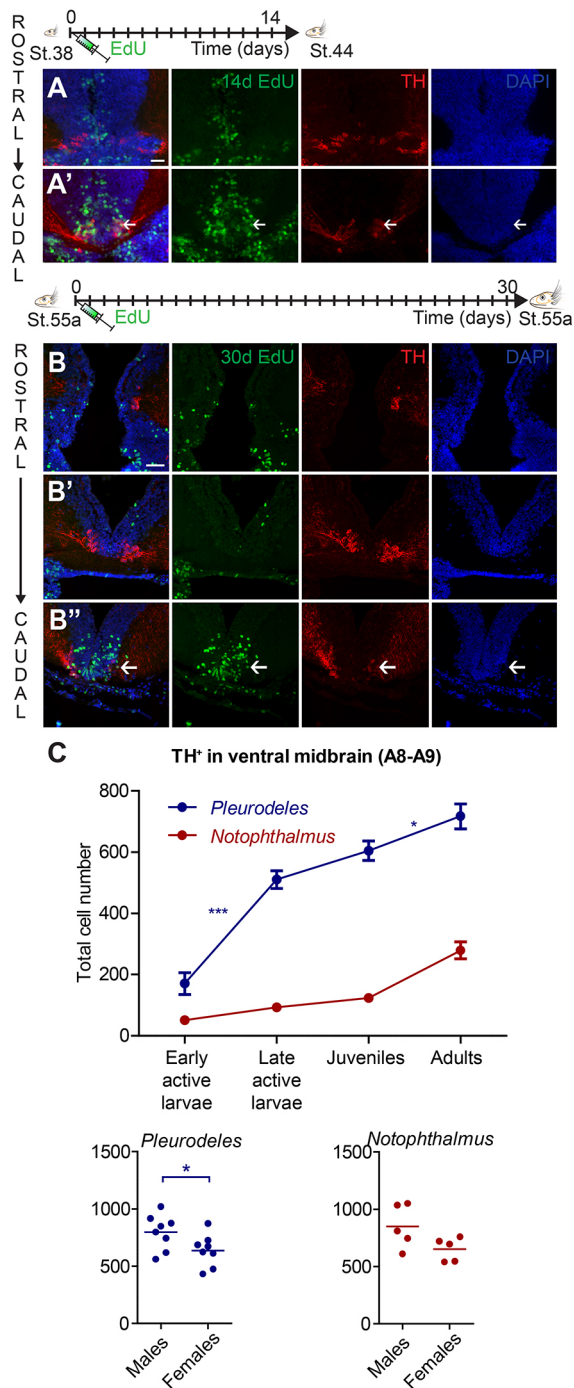
Fig. 5. Dopaminergic and cholinergic neurogenesis: tangential migration, species- and region-specific neuronal growth, and sexual dimorphism. (A,B) EdU pulse-chase experiments indicate tangential migration of precursors during dopaminergic neurogenesis. In both developmental intervals analyzed, EdU$^+$/TH$^+$ cells (arrows) could only be found in the most caudal sections (A′,B″), suggesting a caudal-to-rostral (tangential) migration during dopaminergic neurogenesis in the ventral midbrain. (C) Stereological estimation of total cell number in the dopaminergic subpopulation of the ventral midbrain shows species-specific temporal growth dynamics and sexual dimorphism. The mammalian nomenclature of catecholaminergic cell groups in the neuromeric model (Marin et al., 2005) is indicated within parenthesis (see also Fig. S9). Based on our developmental analysis, the mammillary subpopulation [A14-dm in Marin et al. (2005)] was included in the A10 group (the basal diencephalic group). Cell number during development (top): two-way ANOVA with Bonferroni post-hoc test; *P<0.05, ***P<0.001. Mean±s.e.m. Females versus males (bottom): Student's t-test (two tailed); *P<0.05. Mean±s.e.m. Source data in Tables S28 and S29. Scale bars: 50 µm (A,A′), 100 µm (B-B″).

(Fig. S10D), which lacks comparable dopamine innervation. The average distance was found to be similar in all the groups after a 23 day EdU chase (Fig. 6I), corroborating the transient effect of dopamine depletion on cell proliferation.

DISCUSSION

In this paper, we present a comprehensive analysis of brain formation from larval to adult stages of two salamander model species. We focused on the spatiotemporal dynamics of cell proliferation, ependymoglial differentiation, neurogenesis, neuronal subtype specification and correlated brain maturation with the acquisition of stereotypical behaviors. Our data provide new insights into brain development and evolution in several ways, highlighting both fixed and flexible processes in tetrapods. First, we show that the distribution of proliferative regions is not conserved among closely related species even with very similar overall brain morphology. Second, we show that the cell cycle lengthening during brain ontogeny is a conserved and general attribute in the tetrapod lineage. Third, we show a close correlation between cell cycle lengthening, neurogenesis and ependymoglia maturation. Fourth, we provide a cellular basis for the appearance of higher cognitive functions in salamanders, and reveal that they are evolutionarily conserved among tetrapods.

Similar to other vertebrates, proliferating cells were mainly restricted to the VZ/SVZ at all stages (D'Amico et al., 2011; García-Verdugo et al., 2002; Lam et al., 2009; Lin et al., 2015; Montiel et al., 2016; Moreno and González, 2017). Proliferation in the adult salamander brain has previously been studied during homeostasis, revealing important differences between species. Whereas in adult axolotl proliferation is widespread in many brain regions (Amamoto et al., 2016; Maden et al., 2013; Richter and Kranz, 1981), the adult *Notophthalmus* brain is mainly quiescent (Berg et al., 2010). Here, we found that *Pleurodeles* was more akin to axolotl and also teleost fish in terms of the distribution of germinal zones in the adult brain (Cerri et al., 2009; D'Amico et al., 2011; Ganz and Brand, 2016). Nevertheless, similar to mammals (Faiz et al., 2005), an ontogenetic decline of the proliferation rates is apparent in both *Pleurodeles* and *Notophthalmus*. Our studies here also show that the length of the cell cycle increases during development in both species. These observations are in accordance with the data from other tetrapods showing that cell cycle length extends during brain development (Thuret et al., 2015; Watanabe et al., 2015). Furthermore, the reported values for cell cycle and S-phase lengths in mammals are similar to those we present here (Caviness et al., 1995; Thuret et al., 2015). In the adult *Notophthalmus* brain, two ependymoglial

2010). We observed a similar regenerative response in *Pleurodeles* larvae, which is characterized by an increased number of newborn cells and by the recovery of TH$^+$ neurons (Fig. 6F,G).

We also examined how the absence of dopaminergic innervation affects cell proliferation in the newt forebrain, as lack of dopaminergic innervation in the forebrain has been shown to reduce proliferation and neurogenesis in several mammalian models (Geraerts et al., 2007). In accordance with these reports, we observed a decrease in proliferation in the striatum of injured animals at day 3 (Fig. 6H), an effect that was no longer detected at later time points analyzed (Fig. S10C). After 11 days of EdU chase, the average migration distance was found to be shorter in the striatum of the injured group (Fig. 6I), but not in the medial pallium
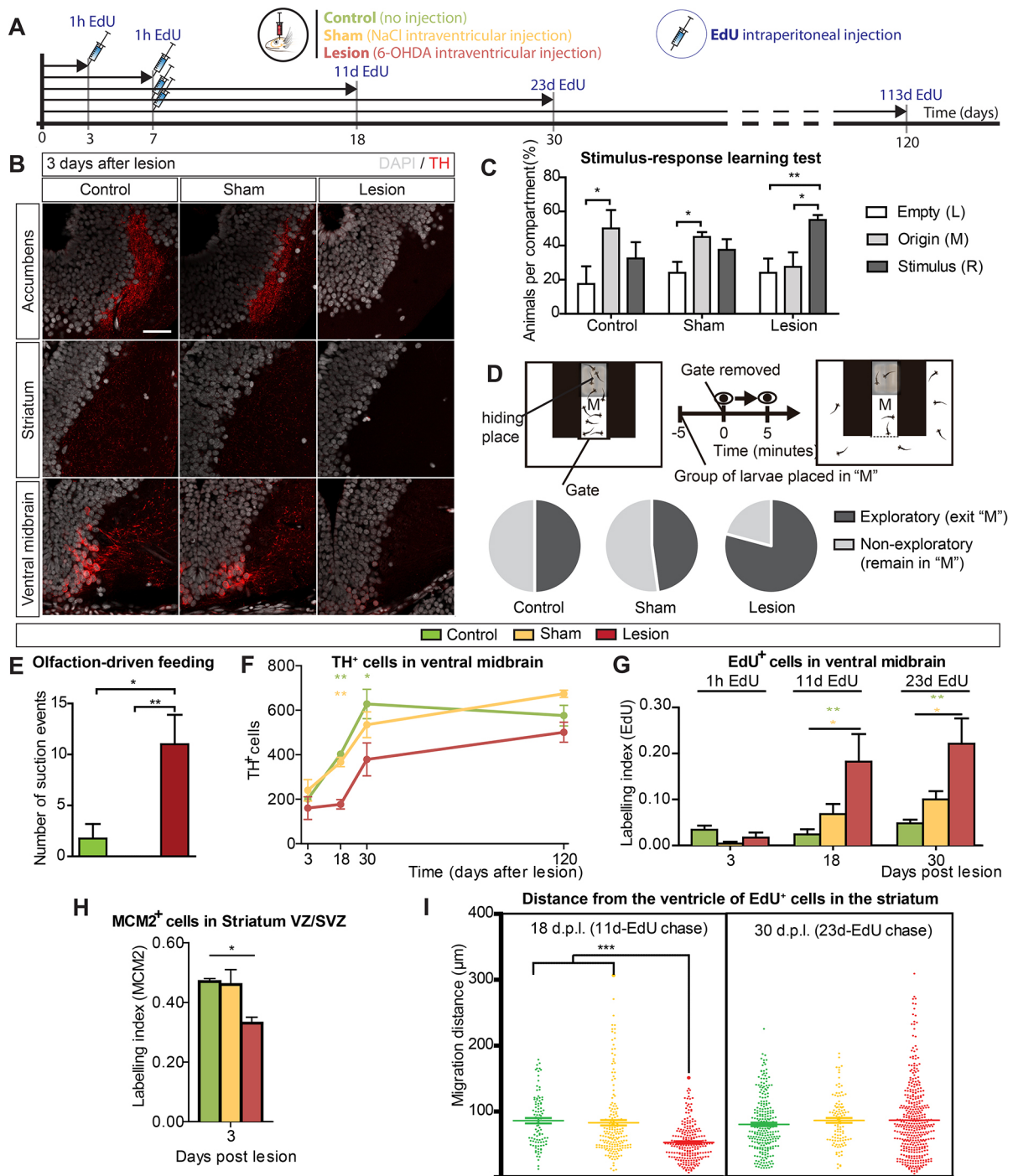
Fig. 6. Functional perturbation of the dopaminergic system alters behavioral performance and neurogenesis. (A) Timeline of the chemical ablation experiment. (B) Representative sections showing ablation of dopaminergic fibers in the forebrain and the corresponding cell bodies in the ventral midbrain. (C) Stimulus response-learning test (see Fig. 4E) performed in 3 cm larvae shows more injured larvae in the chamber with *Artemia*. (D) Fear was tested by placing the animals in a novel environment in the absence of cues. More dopamine-ablated animals are exploratory compared with control and sham injection animals. (E) Suction behavior dramatically increases in the lesion group while performing the olfaction-driven foraging test (see Fig. 4F) in 5 cm animals. (F) Quantification of total cell number in the dopaminergic population of the ventral midbrain shows dopaminergic regeneration. (G) EdU pulse-chase experiment shows an increase in the number of newborn cells in the ventral midbrain in the lesion group. (H) Proliferation is reduced in the striatum of injured larvae. (I) The migration distance of EdU-chased cells is reduced in the striatum of dopamine-depleted animals. *$P<0.05$, **$P<0.01$, ***$P<0.001$ by (E,H,I) one-way ANOVA with Newman-Keuls post-hoc test or (C,F,G) two-way ANOVA with Bonferroni post-hoc test. Mean±s.e.m. Source data in Tables S31-S37. d.p.l., days post-lesion. L, left; M, middle; R, right. Scale bar: 100 μm (B).

subtypes have previously been identified: GS⁺ cells with properties of transit amplifying progenitors, and GS⁻ cells with stem cell features (Kirkham et al., 2014). We find here that during ontogeny all ependymoglia cells are GS⁻ initially. More mature GS⁺

ependymoglia appear within regions that are becoming quiescent and have longer cell cycles.

Neuronal subpopulations are specified through a process of precisely timed acquisition of transcriptional programs, and

migration to spatially confined domains (Barber and Pierani, 2016; Bartolini et al., 2013; Kratochwil et al., 2017). Spatial organization of motor circuits relates to defined connectivity patterns and these patterns frequently correlate with specific behavioral functions of motor output (Arber, 2012). In this work we correlated the timing of neurogenesis in different brain areas with the acquisition of stereotyped behaviors. NeuN$^+$ cells appear first during the initial larval period in the midbrain and in the hindbrain where visual/octavolateral cues are centrally processed to trigger the escape response and feeding by suction (Dicke and Roth, 1994). Most of the dopaminergic and cholinergic subpopulations are present at this stage, but they will continue growing in terms of cell number and complexity of innervation in their target areas. During the active larval period, locomotor and feeding behaviors become more sophisticated, which correlates with a substantial increase in cell number in all diencephalic and mesencephalic subpopulations involved in the control of food intake (Ferrario et al., 2016) and locomotion (Dannenberg et al., 2016; Swart et al., 2017). Our results show that the timing of dopaminergic and cholinergic neurogenesis is region and species specific and also sexually dimorphic in *Pleurodeles*. The growth rates were either biphasic or exponential, analogous to those observed in mammalian dopaminergic neurogenesis (Trujillo-Paredes et al., 2016). Sexual dimorphism has been reported in mammalian dopaminergic subpopulations, but in contrast to salamanders, females appear to have more dopaminergic cells than males in all examined regions except the olfactory bulbs (Abel and Rissman, 2012; Bleier et al., 1982; Gillies et al., 2014; Gómez et al., 2007; McArthur et al., 2007). We hypothesize that allometric scaling of different neuronal subpopulations reflect species-specific adaptations to the environment. As an example, TH$^+$ cells in the olfactory bulbs increase during the larval period in *Pleurodeles* but remains low in *Notophthalmus* larval development. The differential increase of TH$^+$ neurons in the olfactory bulb may be related to differences in prey/predator recognition, emotional learning or social behavior (Sullivan et al., 2015).

We explored in detail the maturation of the telencephalon, which is the most complex brain area in terms of segmentation, structural diversity and behavior control. Our observations indicate that the onset of olfaction occurs during the late active larval period in *Pleurodeles*. Accordingly, the TH$^+$ subpopulation in the olfactory bulbs increases from this stage onwards, and a major neurogenic wave occurs in the ventral and lateral pallia. The ventral pallium gives rise to the lateral amygdala, which receives olfactory information in *Pleurodeles* (Moreno and González, 2007). In mammals, the lateral pallium gives rise to the olfactory cortex, and the medial pallium to the hippocampus (Medina and Abellan, 2009; Montiel and Aboitiz, 2015). We found that the neurogenesis also occurs in the medial pallium when animals start to use spatial information, as demonstrated by olfaction-driven exploratory behaviors and stimulus-response learning. We observed a simultaneous neurogenic process in the striatum, which is responsible for motor control, associative learning and motivated behaviors (Hiebert et al., 2014; Palmiter, 2008). It is noteworthy in this context that the medial pallium remains a germinally active zone for longer in *Notophthalmus* than in *Pleurodeles*. This could reflect the abilities of *Notophthalmus* for true navigation, by which they find their home pond from long distances (Phillips et al., 1995). We found that neurogenesis occurs later in the pallidum, concomitant with the onset of decision enactment in foraging behavior in *Pleurodeles*. This is consistent with the integrative functions associated with the pallidal derivatives. The pallidum will give

rise to the medial amygdala, the main secondary vomeronasal center (Moreno and González, 2007), and also to the bed nucleus of the stria terminalis, an evolutionarily conserved integratory center for the control of instinctive reflexes such as ingestion, reproduction and defense (Moreno et al., 2012). Our data highlight a clear sequence of maturation, with neurogenesis occurring first in sensory and motor areas and later in integratory centers. The relatively late maturation of the dorsal pallium indicates that this region has a higher integrative function. In mammals, the embryonic dorsal pallium gives rise to the isocortex (Montiel and Aboitiz, 2015), and our present findings in salamanders support the hypothesis that the evolutionary origin of the isocortex corresponds to an interface of olfactory-hippocampal networks (Aboitiz and Montiel, 2015).

Our dopaminergic depletion studies indicate the importance of the connectivity and neurochemical properties of a given neuronal subpopulation in neurogenesis and behavior. The data presented herein strongly suggest that the basic mechanisms and functions are conserved in the tetrapod lineage. In humans, the striatum underlies stimulus-response learning and mediates decision making (Hiebert et al., 2014), and dopamine in the accumbens may play an important role in fear conditioning (Levita et al., 2002; Martinez et al., 2008). Our results suggest that, like in mammals, the dopaminergic innervation of the striatum and accumbens might play a role in associative learning, decision enactment, and fear behavior in salamanders. Our results resemble those obtained in mammalian genetic parkinsonian models, where animals with decreased nigrostriatal projections were faster than wild-type mice in finding their correct food in a T-maze (Ardayfio et al., 2008; Bissonette and Roesch, 2016). Similar to the outcome of studies performed in rodents and primates (Geraerts et al., 2007), experimental depletion of dopamine leads to reduced proliferation and cell migration in the salamander forebrain.

Our study provides a framework for future research in brain regeneration assessing neurogenic programs and functional recovery of behaviors. The new transgenic lines that we present here also allow precise cell tracking, lineage tracing and clonal analyses. These lines represent important tools, and they can also shed light on mechanisms underlying brain morphogenesis, growth and cell diversification, contributing to the understanding of vertebrate brain evolution.

MATERIALS AND METHODS
Animals
Two salamander species were used in the present study. Adult *Notophthalmus viridescens* were purchased from Charles Sullivan (Nashville, TN, USA). Adult *Pleurodeles waltl* were raised in our colony, except for some 9-year-old animals kindly donated by Jean Marie Cabelguen (Magendie Neurocenter, Inserm U862, Bordeaux, France) and Tiphaine Davit-Béal (Pierre et Marie Curie University, Paris, France). All animals were kept in our facility under standard conditions of 12 h light/12 h darkness at 18-24°C. Animals were maintained, raised and staged according to standard *Pleurodeles* husbandry protocols, and eggs were obtained from natural/hormone-induced breeding (Joven et al., 2015), with minor modifications for the eft phase of *Notophthalmus* (diet based on live food purchased from www.dartfrog.co.uk). All experiments were performed according to local and European ethical permits.

Tissue processing
Prior to fixation by immersion/perfusion with MEMFA (0.1 M MOPS pH 7.6, 2 mM EGTA, 1 mM MgSO$_4$, 3.7% formaldehyde), animals were deeply anesthetized by immersion in a solution of MS222 (Sigma) at a range of concentrations (0.02% for larvae, 0.5% for efts and large *Pleurodeles* larvae, 0.1% for adult *Notophthalmus* and postmetamorphic *Pleurodeles*, 0.2% for adult *Pleurodeles*). Brains were dissected out and kept in the same fixative solution for 3-12 h at 4°C. After fixation, the brains were immersed in a solution of 30% sucrose in DPBS (HyClone) until they sank. Tissue was

pre-embedded at 37°C overnight in 3.5% gelatin with 30% sucrose in DPBS, then embedded in 7.5% gelatin with 30% sucrose in DPBS, and quickly frozen with dry ice. Sections of 20-30 μm were prepared on a cryostat at −30°C (Leica, CM3050S) in the transverse, sagittal or horizontal planes, collected on SuperFrost slides (Thermo Scientific Menzel Gläser Superfrost Plus) in three to five series depending on the sample size. Slides were immediately processed or stored at −80°C until use.

Staining procedures
Immunohistochemistry was performed as previously described using primary antibodies against highly conserved proteins, most of them previously tested in *Pleurodeles* and *Notophthalmus* (Table S1), with some minor modifications: after sealing the edges with a hydrophobic barrier pen (ImmEdge), gelatin was washed out of the slides by either PBS at 37°C for 30 min or by antigen retrieval, for which slides were immersed in citrate buffer pH 6 (10 mM sodium citrate dehydrate, Sigma) for 25 min at 70°C, followed by 25 min at room temperature. Subsequently, slides were washed twice for 10 min each in PBS containing 0.2% Triton X-100 (Tx, Sigma) followed by a last wash in PBS for 10 min (this washing procedure was repeated after every incubation). All sections were blocked in blocking solutions comprising either 5% donkey serum and 0.2% Tx in PBS, or 0.2% BSA, 0.2% fish skin gelatin (Sigma) and 0.2% Tx in PBS for 0.5-3 h at room temperature. For incubation, slides were placed in a home-made humidity chamber on a shaker to ensure that the whole surface of each slide was equally exposed to the antibodies. Primary antibodies were diluted in PBS/0.2% Tx at the desired concentration and slides were incubated for 12-24 h at room temperature. Secondary antibodies were diluted 1:500 in PBS/0.2% Tx and slides incubated for 1.5-3 h at room temperature. The conjugated primary antibody GFAP-cy3 was added after fixation of stained material followed by another round of blocking. EdU staining was performed after immunohistochemistry by incubating sections with 100 mM Tris pH 8.5, 1 mM CuSO$_4$, 50-100 μM fluorescent azide, and 100 mM ascorbic acid as prescribed (Salic and Mitchison, 2008). For BrdU immunohistochemistry, sections were first stained for other desired markers and with DAPI, then fixed in 4% PFA for 1-2 min at room temperature, followed by 2 M HCl/0.5% Tx treatment (15-20 min at 37°C), and then incubation in primary and secondary antibodies.

Thymidine analog injections and estimation of cell cycle length
EdU and BrdU were administrated intraperitoneally (50 mg/kg body weight). Adult newts and large larvae (from 4 cm long, stage 55a onwards) were injected with a syringe. Larvae up to 4 cm were placed on wet paper under anesthesia, quickly microinjected by FemtoJet (Eppendorf), and immediately returned to water. Microinjections were performed using a small animal stereotactic device adapted for neonatal mouse and rodents with a V-clamp to hold a probe, to which the universal capillary holder arm of the FemtoJet was attached. In order to control the volume of injection, 1 mm divisions were previously marked in the glass needles obtained by pulling borosilicate glass capillaries (Harvard Apparatus, GC100F-10) with a Flaming/Brown type micropipette puller (P-97, Sutter Instrument). Needles were filled using Femtotips (Eppendorf).

For the cell cycle length estimation, animals were kept individually and placed in anesthesia 10 min before being injected and sacrificed at strict times: EdU injection ($t=0$), BrdU injection ($t=1.5$ h), sacrifice ($t=2$ h). Stainings were performed as described in the previous section in the following order: Sox2 immunostaining, EdU detection, fixation, HCl treatment and BrdU immunostaining. The exact number of proliferating cells (MCM2 labeling index in VZ/SVZ) was calculated for each case (species, stage and region) using the adjacent series. Quantification on confocal images allowed estimation of the total length of S-phase (Table S17) and of the cell cycle (Table S18) in neural stem/progenitors (Martynoga et al., 2005; Nowakowski et al., 1989): S=EdU$^+$/BrdU$^+$ cells; L=EdU$^+$/BrdU$^-$ cells; P=proliferating cells [Sox2$^+$ cells×MCM2 labeling index (L.I.)]; Ti=time of incorporation (1.5 h); Ts (S-phase)=Ti/(L/S); and Tc (cell cycle length)=Ts/(S/P).

Plasmids
The *CMV-H2bYFP* plasmid was from Berg et al. (2011); the *CAGGS:loxp-Cherry-STOP-loxp-H2BYFP* and *CAGGS:loxp-GFP-STOP-loxp-Cherry*

plasmids were from Sandoval-Guzman et al. (2014); Nucbow (*Nuc*), Cytbow (*Cyt*) and self-excising Cre (*seCre*) plasmids were from Loulier et al. (2014). Plasmids were purified using Qiagen Maxiprep and were resuspended in 10 mM Tris-HCl (pH 8.5).

Electroporation
Intraventricular injections of the plasmids were performed on anesthetized animals, with prior drilling of the skull with a Tungsten carbon dental bur with a round head 0.5 mm in diameter in the case of postmetamorphic newts as previously described (Kirkham and Joven, 2015). Electroporations were performed towards the ventral or lateral walls of the ventricle with a NEPA21 electroporator (Nepagene) using tweezers with round platinum plate electrodes 5 mm in diameter (Nepagene, CUY650P5) as described previously (Kirkham and Joven, 2015) for the postmetamorphic animals, and following the method of spinal cord electroporation developed for axolotl (Rodrigo Albors and Tanaka, 2015) with some modifications for the larvae: animals were placed in a 2% agarose carved mold filled with ice-cold MS-222, with the distance between electrodes being 7 mm (Fig. S3A). In order to optimize electroporation outcome, a range of conditions was used for the latter; we observed that a freshly made agarose chamber, plasmid diluted in PBS and small size of larvae showed better results in terms of a greater density of electroporated cells. The newts were electroporated in a unidirectional (+) manner, as bidirectional (+/−) pulses resulted in the majority of electroporated cells being placed still on one side. The machine was set to give one pore-forming pulse at 50 ms on and 95 ms off, followed by five 50 ms transfer pulses with 950-999 ms gap between each pulse. Pore-forming pulses ranged from 50 mV/cm to 135 mV/cm, and transfer pulses from 40 mV/cm to 75 mV/cm with a decay of 5% between the pulses. The specific conditions used for the experiments shown in the figures are given in Tables S7-S15.

Transgenesis
The *Pw$^{GFP-loxp-Cherry}$* transgenic newts were generated via I-*Sce*I meganuclease enzyme (NEB)-assisted plasmid injection as described previously (Khattak et al., 2013). A combination of *Nuc* and *Cyt* plasmids were injected into single-cell eggs together with Tol2 transposase to generate transgenic *Pleurodeles waltl* carrying the brainbow transgenes (*Pw^{NucCyt}*) as previously described for axolotl (Khattak et al., 2014; Khattak and Tanaka, 2015). Tol2 transposase was made according to Khattak et al. (2014). We performed pilot experiments in the F0 generation to ensure the correct functioning of the loxP system, but we observed different degrees of mosaicism in the founder generation (data not shown). Therefore, only the positive offspring (F1) were used for further experiments, after being screened using a fluorescence inverted microscope.

Behavioral observations
Videos of different developmental stages were recorded with a Sony Xperia X Compact F5321 smartphone. The movies were mounted and edited with Movie Maker (Microsoft), and then compressed with the open source video transcoder Handbrake. In order to assess olfaction, motivational modulation of locomotor behavior (stimulus-response learning) and olfaction-driven foraging behavior, we manufactured a modified T-maze in which animals were exposed to different cues before feeding (frozen bloodworm infusion, *Artemia*, or filter bag with frozen bloodworms). Aquarium filter foam was cut with a scalpel to create a three-chambered tri-dimensional space. Before every observation, the foam was washed and inserted in one of the housing tanks filled with the appropriate volume of new water. Animals were placed in the middle chamber, and 5 min later the gate was opened and the cues added. Groups of small larvae (up to 3 cm long) were counted 5 min after cue exposure (Tables S23, S24 and S31). Individual late active larvae (5 cm long) were continuously observed during 10 min (Table S25), and average time and feeding events were calculated (Tables S26, S27 and S33). To test fear, we placed the animals in a new environment including a hiding area, without additional stimuli. During 5 min we observed the exploratory/hiding behavior, and quantified the number of animals exiting the middle chamber (Table S32).

Dopaminergic chemical ablation
We adopted the midbrain dopaminergic lesion paradigm by intraventricular injection of the neurotoxin 6-OHDA (Parish et al., 2007). A 0.6 mg/ml

solution of 6-OHDA was kept on ice until the time of injection. We followed the microinjection procedure described for thymidine analog injections, except that the injections were performed intraventricularly at the level of the midbrain. We injected 3 mg of neurotoxin per gram of larval weight. Sham injured animals were injected with the same volume of 0.9% saline. Absence of TH^+ fibers in the striatum of 6-OHDA-injured animals and counting of TH^+ neurons in the ventral midbrain (Table S34) revealed that we were able to obtain consistent bilateral lesions of the dopaminergic cell groups of interest.

Imaging

A Leica M80 stereomicroscope equipped with a Leica IC80HD camera was used for dissecting and imaging brains. Transgenic embryos and larvae were screened and imaged using a Zeiss Axiovert 200 M inverted microscope. Slides were examined with Zeiss upright (Axio Imager Z2) and confocal (LSM 700, LSM 880) microscopes. All microscopes were equipped with fluorescence illumination (HXP120V, HXP120C) and images were taken using ZEN software (Zeiss). Images were subsequently processed for brightness and contrast adjustments and for evaluation and presentation of the results using Adobe Photoshop or ImageJ. Microsoft Excel and GraphPad Prism were used to generate graphs. Schematic drawings and final figures were prepared using Adobe Illustrator.

Quantification and stereology

All countings were performed in serial sections. Detailed information about developmental stages and n values for the different experiments that involved quantification of cells or measurements of distances and tissue thickness is available in Tables S2-S6, S16-S22, S28-S30 and S34-S38. The results presented correspond to the average of the values obtained from n biological replicates. In general, n represents the number of animals, except for Tables S19-S22 and for S37, S38, where n represents the number of sections (one animal per group) and cells (pooled from three or four different animals per group), respectively. Estimation of total TH^+ or $ChAT^+$ cell number in the different subpopulations (Tables S28-S30 and S34) was obtained by counting, in an upright microscope equipped with fluorescence illumination, the total number of cells in 20-30 μm serial sections, then the values were multiplied by the number of series in each case. Labeling indexes and percentages (Tables S2-S6, S35 and S36) were calculated by dividing the number of labeled cells of interest by total cell nuclei (for percentages, labeling index values were multiplied by 100) from confocal images, obtained by systematic random sampling in well-defined regions of interest based on anatomical landmarks (optical fractionator method).

Statistical analyses

In figures, mean values and standard error bars are shown. P-values are provided where appropriate in the supplementary information. Student's t-test was performed in Microsoft Excel. One-way ANOVA with Newman-Keuls post-hoc tests and two-way ANOVA with Bonferroni post-hoc tests were performed in GraphPad Prism.

Competing interests

The authors declare no competing or financial interests.

Author contributions

Conceptualization: A.J., A.S.; Methodology: A.J., H.W., L.S.H.; Formal analysis: A.J., T.P., L.S.H., L.B.; Investigation: A.J., H.W., T.P., L.S.H., L.B.; Resources: A.J., H.W., A.S.; Data curation: A.J.; Writing - original draft: A.J.; Writing - review & editing: A.J., A.S.; Visualization: A.J.; Supervision: A.J., A.S.; Project administration: A.S.; Funding acquisition: A.S.

Supplementary information

Supplementary information available online at
http://dev.biologists.org/lookup/doi/10.1242/dev.160051.supplemental

References

Abel, J. L. B. and Rissman, E. F. (2012). Location, location, location: genetic regulation of neural sex differences. *Rev. Endocr. Metab. Disord.* **13**, 151-161.

Aboitiz, F. and Montiel, J. F. (2015). Olfaction, navigation, and the origin of isocortex. *Front. Neurosci.* **9**, 402.

Abraham, A. D., Neve, K. A. and Lattal, K. M. (2014). Dopamine and extinction: a convergence of theory with fear and reward circuitry. *Neurobiol. Learn. Mem.* **108**, 65-77.

Amamoto, R., Huerta, V. G., Takahashi, E., Dai, G., Grant, A. K., Fu, Z. Arlotta, P. (2016). Adult axolotls can regenerate original neuronal diversity in response to brain injury. *eLife* **5**, e13998.

Arber, S. (2012). Motor circuits in action: specification, connectivity, and function. *Neuron* **74**, 975-989.

Ardayfio, P., Moon, J., Leung, K. K. A., Youn-Hwang, D. and Kim, K.-S. (2008). Impaired learning and memory in Pitx3 deficient aphakia mice: a genetic model for striatum-dependent cognitive symptoms in Parkinson's disease. *Neurobiol. Dis.* **31**, 406-412.

Barber, M. and Pierani, A. (2016). Tangential migration of glutamatergic neurons and cortical patterning during development: Lessons from Cajal-Retzius cells. *Dev. Neurobiol.* **76**, 847-881.

Barbosa, J. S., Sanchez-Gonzalez, R., Di Giaimo, R., Baumgart, E. V., Theis, F. J., Gotz, M. and Ninkovic, J. (2015). Neurodevelopment. Live imaging of adult neural stem cell behavior in the intact and injured zebrafish brain. *Science* **348**, 789-793.

Bartolini, G., Ciceri, G. and Marín, O. (2013). Integration of GABAergic interneurons into cortical cell assemblies: lessons from embryos and adults. *Neuron* **79**, 849-864.

Berg, D. A., Kirkham, M., Beljajeva, A., Knapp, D., Habermann, B., Ryge, J., Tanaka, E. M. and Simon, A. (2010). Efficient regeneration by activation of neurogenesis in homeostatically quiescent regions of the adult vertebrate brain. *Development* **137**, 4127-4134.

Berg, D. A., Kirkham, M., Wang, H., Frisén, J. and Simon, A. (2011). Dopamine controls neurogenesis in the adult salamander midbrain in homeostasis and during regeneration of dopamine neurons. *Cell Stem Cell* **8**, 426-433.

Bissonette, G. B. and Roesch, M. R. (2016). Development and function of the midbrain dopamine system: what we know and what we need to. *Genes Brain Behav.* **15**, 62-73.

Bleier, R., Byne, W. and Siggelkow, I. (1982). Cytoarchitectonic sexual dimorphisms of the medial preoptic and anterior hypothalamic areas in guinea pig, rat, hamster, and mouse. *J. Comp. Neurol.* **212**, 118-130.

Caviness, V. S., Jr, Takahashi, T. and Nowakowski, R. S. (1995). Numbers, time and neocortical neuronogenesis: a general developmental and evolutionary model. *Trends Neurosci.* **18**, 379-383.

Cerri, S., Bottiroli, G., Bottone, M. G., Barni, S. and Bernocchi, G. (2009). Cell proliferation and death in the brain of active and hibernating frogs. *J. Anat.* **215**, 124-131.

Charvet, C. J., Striedter, G. F. and Finlay, B. L. (2011). Evo-devo and brain scaling: candidate developmental mechanisms for variation and constancy in vertebrate brain evolution. *Brain Behav. Evol.* **78**, 248-257.

Coghill, G. E. (1924). Correlated anatomical and physiological studies of the growth of the nervous system of Amphibia. IV. Rates of proliferation and differentiation in the central nervous system of Amblystoma. *J. Comp. Neurol.* **37**, 71-120.

D'Amico, L. A., Boujard, D. and Coumailleau, P. (2011). Proliferation, migration and differentiation in juvenile and adult Xenopus laevis brains. *Brain Res.* **1405**, 31-48.

Dannenberg, H., Hinman, J. R. and Hasselmo, M. E. (2016). Potential roles of cholinergic modulation in the neural coding of location and movement speed. *J. Physiol. Paris* **110**, 52-64.

Dicke, U. and Roth, G. (1994). Tectal activation of premotor and motor networks during feeding in salamanders. *Eur. J. Morphol.* **32**, 106-116.

Faiz, M., Acarin, L., Castellano, B. and Gonzalez, B. (2005). Proliferation dynamics of germinative zone cells in the intact and excitotoxically lesioned postnatal rat brain. *BMC Neurosci.* **6**, 26.

Fareri, D. S. and Tottenham, N. (2016). Effects of early life stress on amygdala and striatal development. *Dev. Cogn. Neurosci.* **19**, 233-247.

Fentress, J. C. (1992). Emergence of pattern in the development of mammalian movement sequences. *J. Neurobiol.* **23**, 1529-1556.

Ferrario, C. R., Labouèbe, G., Liu, S., Nieh, E. H., Routh, V. H., Xu, S. and O'Connor, E. C. (2016). Homeostasis meets motivation in the battle to control food intake. *J. Neurosci.* **36**, 11469-11481.

Ganz, J. and Brand, M. (2016). Adult neurogenesis in fish. *Cold Spring Harb. Perspect. Biol.* **8**, a019018.

García-Verdugo, J. M., Ferrón, S., Flames, N., Collado, L. A., Desfilis, E. and Font, E. (2002). The proliferative ventricular zone in adult vertebrates: a comparative study using reptiles, birds, and mammals. *Brain Res. Bull.* **57**, 765-775.

Geraerts, M., Krylyshkina, O., Debyser, Z. and Baekelandt, V. (2007). Concise review: therapeutic strategies for Parkinson disease based on the modulation of adult neurogenesis. *Stem Cells* **25**, 263-270.

Gillies, G. E., Virdee, K., McArthur, S. and Dalley, J. W. (2014). Sex-dependent diversity in ventral tegmental dopaminergic neurons and developmental programing: a molecular, cellular and behavioral analysis. *Neuroscience* **282**, 69-85.

Gómez, C., Briñón, J. G., Valero, J., Recio, J. S., Murias, A. R., Curto, G. G., Orio, L., Colado, M. I. and Alonso, J. R. (2007). Sex differences in catechol contents in the olfactory bulb of control and unilaterally deprived rats. *Eur. J. Neurosci.* **25**, 1517-1528.

Griffiths, R. (1995). *Newts and Salamanders of Europe.* London: Poyser Natural History.

Hamburger, V. (1963). Some aspects of the embryology of behavior. *Q. Rev. Biol.* **38**, 342-365.

Hameed, L. S., Berg, D. A., Belnoue, L., Jensen, L. D., Cao, Y. and Simon, A. (2015). Environmental changes in oxygen tension reveal ROS-dependent neurogenesis and regeneration in the adult newt brain. *eLife* **4**, e08422.

Hiebert, N. M., Vo, A., Hampshire, A., Owen, A. M., Seergobin, K. N. and MacDonald, P. A. (2014). Striatum in stimulus–response learning via feedback and in decision making. *Neuroimage* **101**, 448-457.

Joven, A., Morona, R., González, A. and Moreno, N. (2013a). Expression patterns of Pax6 and Pax7 in the adult brain of a urodele amphibian, Pleurodeles waltl. *J. Comp. Neurol.* **521**, 2088-2124.

Joven, A., Morona, R., González, A. and Moreno, N. (2013b). Spatiotemporal patterns of Pax3, Pax6, and Pax7 expression in the developing brain of a urodele amphibian, Pleurodeles waltl. *J. Comp. Neurol.* **521**, 3913-3953.

Joven, A., Kirkham, M. and Simon, A. (2015). Husbandry of Spanish ribbed newts (Pleurodeles waltl). *Methods Mol. Biol.* **1290**, 47-70.

Kaslin, J., Ganz, J. and Brand, M. (2008). Proliferation, neurogenesis and regeneration in the non-mammalian vertebrate brain. *Philos. Trans. R. Soc. Lond. B Biol. Sci.* **363**, 101-122.

Khattak, S. and Tanaka, E. M. (2015). Transgenesis in axolotl (Ambystoma mexicanum). *Methods Mol. Biol.* **1290**, 269-277.

Khattak, S., Schuez, M., Richter, T., Knapp, D., Haigo, S. L., Sandoval-Guzmán, T., Hradlikova, K., Duemmler, A., Kerney, R. and Tanaka, E. M. (2013). Germline transgenic methods for tracking cells and testing gene function during regeneration in the axolotl. *Stem Cell Rep.* **1**, 90-103.

Khattak, S., Murawala, P., Andreas, H., Kappert, V., Schuez, M., Sandoval-Guzmán, T., Crawford, K. and Tanaka, E. M. (2014). Optimized axolotl (Ambystoma mexicanum) husbandry, breeding, metamorphosis, transgenesis and tamoxifen-mediated recombination. *Nat. Protoc.* **9**, 529-540.

Kirkham, M. and Joven, A. (2015). Studying newt brain regeneration following subtype specific neuronal ablation. *Methods Mol. Biol.* **1290**, 91-99.

Kirkham, M., Hameed, L. S., Berg, D. A., Wang, H. and Simon, A. (2014). Progenitor cell dynamics in the Newt Telencephalon during homeostasis and neuronal regeneration. *Stem Cell Rep.* **2**, 507-519.

Kratochwil, C. F., Maheshwari, U. and Rijli, F. M. (2017). The long journey of pontine nuclei neurons: from rhombic lip to cortico-ponto-cerebellar circuitry. *Front. Neural Circuits* **11**, 33.

Lam, C. S., März, M. and Strähle, U. (2009). gfap and nestin reporter lines reveal characteristics of neural progenitors in the adult zebrafish brain. *Dev. Dyn.* **238**, 475-486.

Levita, L., Dalley, J. W. and Robbins, T. W. (2002). Nucleus accumbens dopamine and learned fear revisited: a review and some new findings. *Behav. Brain Res.* **137**, 115-127.

Lin, R., Cai, J., Nathan, C., Wei, X., Schleidt, S., Rosenwasser, R. and Iacovitti, L. (2015). Neurogenesis is enhanced by stroke in multiple new stem cell niches along the ventricular system at sites of high BBB permeability. *Neurobiol. Dis.* **74**, 229-239.

Loulier, K., Barry, R., Mahou, P., Le Franc, Y., Supatto, W., Matho, K. S., Ieng, S., Fouquet, S., Dupin, E., Benosman, R. et al. (2014). Multiplex cell and lineage tracking with combinatorial labels. *Neuron* **81**, 505-520.

Maden, M., Manwell, L. A. and Ormerod, B. K. (2013). Proliferation zones in the axolotl brain and regeneration of the telencephalon. *Neural Dev.* **8**, 1.

Marin, F., Herrero, M.-T., Vyas, S. and Puelles, L. (2005). Ontogeny of tyrosine hydroxylase mRNA expression in mid- and forebrain: neuromeric pattern and novel positive regions. *Dev. Dyn.* **234**, 709-717.

Martinez, R. C. R., Oliveira, A. R., Macedo, C. E., Molina, V. A. and Brandão, M. L. (2008). Involvement of dopaminergic mechanisms in the nucleus accumbens core and shell subregions in the expression of fear conditioning. *Neurosci. Lett.* **446**, 112-116.

Martynoga, B., Morrison, H., Price, D. J. and Mason, J. O. (2005). Foxg1 is required for specification of ventral telencephalon and region-specific regulation of dorsal telencephalic precursor proliferation and apoptosis. *Dev. Biol.* **283**, 113-127.

McArthur, S., McHale, E. and Gillies, G. E. (2007). The size and distribution of midbrain dopaminergic populations are permanently altered by perinatal glucocorticoid exposure in a sex- region- and time-specific manner. *Neuropsychopharmacology* **32**, 1462-1476.

Medina, L. and Abellán, A. (2009). Development and evolution of the pallium. *Semin. Cell Dev. Biol.* **20**, 698-711.

Montgomery, S. H., Mundy, N. I. and Barton, R. A. (2016). Brain evolution and development: adaptation, allometry and constraint. *Proc. Biol. Sci.* **283**, 20160433.

Montiel, J. F. and Aboitiz, F. (2015). Pallial patterning and the origin of the isocortex. *Front. Neurosci.* **9**, 377.

Montiel, J. F., Vasistha, N. A., Garcia-Moreno, F. and Molnár, Z. (2016). From sauropsids to mammals and back: New approaches to comparative cortical development. *J. Comp. Neurol.* **524**, 630-645.

Moreno, N. and González, A. (2007). Regionalization of the telencephalon in urodele amphibians and its bearing on the identification of the amygdaloid complex. *Front. Neuroanat.* **1**, 1.

Moreno, N. and González, A. (2017). Pattern of neurogenesis and identification of neuronal progenitor subtypes during pallial development in Xenopus laevis. *Front. Neuroanat.* **11**, 24.

Moreno, N., Morona, R., López, J. M., Dominguez, L., Joven, A., Bandin, S. and González, A. (2012). Characterization of the bed nucleus of the stria terminalis in the forebrain of anuran amphibians. *J. Comp. Neurol.* **520**, 330-363.

Nomura, T., Gotoh, H. and Ono, K. (2013). Changes in the regulation of cortical neurogenesis contribute to encephalization during amniote brain evolution. *Nat. Commun.* **4**, 2206.

Nomura, T., Ohtaka-Maruyama, C., Yamashita, W., Wakamatsu, Y., Murakami, Y., Calegari, F., Suzuki, K., Gotoh, H. and Ono, K. (2016). The evolution of basal progenitors in the developing non-mammalian brain. *Development* **143**, 66-74.

Nowakowski, R. S., Lewin, S. B. and Miller, M. W. (1989). Bromodeoxyuridine immunohistochemical determination of the lengths of the cell cycle and the DNA-synthetic phase for an anatomically defined population. *J. Neurocytol.* **18**, 311-318.

O'Connell, L. A. (2013). Evolutionary development of neural systems in vertebrates and beyond. *J. Neurogenet.* **27**, 69-85.

Palmiter, R. D. (2008). Dopamine signaling in the dorsal striatum is essential for motivated behaviors: lessons from dopamine-deficient mice. *Ann. N. Y. Acad. Sci.* **1129**, 35-46.

Parish, C. L., Beljajeva, A., Arenas, E. and Simon, A. (2007). Midbrain dopaminergic neurogenesis and behavioural recovery in a salamander lesion-induced regeneration model. *Development* **134**, 2881-2887.

Phillips, J. B., Adler, K. and Borland, S. C. (1995). True navigation by an amphibian. *Anim. Behav.* **50**, 855-858.

Raucci, F., Di Fiore, M. M., Pinelli, C., D'Aniello, B., Luongo, L., Polese, G. and Rastogi, R. K. (2006). Proliferative activity in the frog brain: a PCNA-immunohistochemistry analysis. *J. Chem. Neuroanat.* **32**, 127-142.

Richter, W. and Kranz, D. (1981). Autoradiographic investigations on postnatal proliferative activity of the telencephalic and diencephalic matrix-zones in the axolotl (Ambystoma mexicanum), with special references to the olfactory organ. *Zeitschrift fur mikroskopisch-anatomische Forschung* **95**, 883-904.

Rodrigo Albors, A. and Tanaka, E. M. (2015). High-efficiency electroporation of the spinal cord in larval axolotl. *Methods Mol. Biol.* **1290**, 115-125.

Roth, G. and Walkowiak, W. (2015). The influence of genome and cell size on brain morphology in amphibians. *Cold Spring Harb. Perspect. Biol.* **7**, a019075.

Roth, G., Nishikawa, K. C., Naujoks-Manteuffel, C., Schmidt, A. and Wake, D. B. (1993). Paedomorphosis and simplification in the nervous system of salamanders. *Brain Behav. Evol.* **42**, 137-170.

Salic, A. and Mitchison, T. J. (2008). A chemical method for fast and sensitive detection of DNA synthesis in vivo. *Proc. Natl. Acad. Sci. USA* **105**, 2415-2420.

Sandoval-Guzmán, T., Wang, H., Khattak, S., Schuez, M., Roensch, K., Nacu, E., Tazaki, A., Joven, A., Tanaka, E. M. and Simon, A. (2014). Fundamental differences in dedifferentiation and stem cell recruitment during skeletal muscle regeneration in two salamander species. *Cell Stem Cell* **14**, 174-187.

Sullivan, R. M., Wilson, D. A., Ravel, N. and Mouly, A. M. (2015). Olfactory memory networks: from emotional learning to social behaviors. *Front. Behav. Neurosci.* **9**, 36.

Swart, J. C., Frobose, M. I., Cook, J. L., Geurts, D. E., Frank, M. J., Cools, R. and den Ouden, H. E. (2017). Catecholaminergic challenge uncovers distinct Pavlovian and instrumental mechanisms of motivated (in)action. *eLife* **6**, e22169.

Takeuchi, K., Sereemaspun, A., Inagaki, T., Hakamata, Y., Kaneko, T., Murakami, T., Takahashi, M., Kobayashi, E. and Ookawara, S. (2003). Morphologic characterization of green fluorescent protein in embryonic, neonatal, and adult transgenic rats. *Anat. Rec. A Discov. Mol. Cell. Evol. Biol.* **274A**, 883-886.

Thuret, R., Auger, H. and Papalopulu, N. (2015). Analysis of neural progenitors from embryogenesis to juvenile adult in Xenopus laevis reveals biphasic neurogenesis and continuous lengthening of the cell cycle. *Biol. Open* **4**, 1772-1781.

Trujillo-Paredes, N., Valencia, C., Guerrero-Flores, G., Arzate, D.-M., Baizabal, J.-M., Guerra-Crespo, M., Fuentes-Hernandez, A., Zea-Armenta, I. and Covarrubias, L. (2016). Regulation of differentiation flux by Notch signalling influences the number of dopaminergic neurons in the adult brain. *Biol. Open* **5**, 336-347.

DEVELOPMENT

Watanabe, N., Kageyama, R. and Ohtsuka, T. (2015). Hbp1 regulates the timing of neuronal differentiation during cortical development by controlling cell cycle progression. *Development* **142**, 2278-2290.

Wullimann, M. F., Rink, E., Vernier, P. and Schlosser, G. (2005). Secondary neurogenesis in the brain of the African clawed frog, Xenopus laevis, as revealed by PCNA, Delta-1, Neurogenin-related-1, and NeuroD expression. *J. Comp. Neurol.* **489**, 387-402.

Zupanc, G. K. H., Hinsch, K. and Gage, F. H. (2005). Proliferation, migration, neuronal differentiation, and long-term survival of new cells in the adult zebrafish brain. *J. Comp. Neurol.* **488**, 290-319.

DEVELOPMENT